

# Effect of non-local correlations on the electronic structure of LiFeAs

Karim Zantout,<sup>1,\*</sup> Steffen Backes,<sup>2</sup> and Roser Valentí<sup>1</sup>

<sup>1</sup>*Institut für Theoretische Physik, Goethe-Universität Frankfurt, 60438 Frankfurt am Main, Germany*

<sup>2</sup>*CPHT, CNRS, Institut Polytechnique de Paris, F-91128 Palaiseau, France*

We investigate the role of non-local correlations in LiFeAs by exploring an ab-initio-derived multi-orbital Hubbard model for LiFeAs via the Two-Particle Self-Consistent (TPSC) approach. The multi-orbital formulation of TPSC approximates the irreducible interaction vertex to be an orbital-dependent constant, which is self-consistently determined from local spin and charge sum rules. Within this approach, we disentangle the contribution of local and non-local correlations in LiFeAs and show that in the local approximation one recovers the dynamical-mean field theory (DMFT) result. The comparison of our theoretical results to most recent angular-resolved photoemission spectroscopy (ARPES) and de-Haas van Alphen (dHvA) data shows that non-local correlations in LiFeAs are decisive to describe the measured spectral function  $A(\vec{k}, \omega)$ , Fermi surface and scattering rates. These findings underline the importance of non-local correlations and benchmark different theoretical approaches for iron-based superconductors.

**Introduction.-** The nature of the electronic structure in iron-based superconductors has been intensively scrutinized since their discovery in 2008<sup>1,2</sup>. While *ab initio* density functional theory (DFT) calculations can provide a qualitative understanding of their bandstructure and Fermi surface<sup>3-5</sup>, it became soon evident that correlation effects originating from the strong local Coulomb repulsion on the Fe atoms are responsible for many experimental findings such as large effective masses, Fermi surface renormalization, finite lifetimes or transfer of spectral weight to high binding energies<sup>6-20</sup>. The combined DFT with Dynamical Mean Field Theory (DFT+DMFT) method, which approximates the electronic self-energy to be local in space and thus includes frequency- and orbital-dependent local effects of electronic correlations, has been very successful in capturing many of these observations. Some examples are orbital-dependent correlations, incoherence properties and Fermi surface renormalization.<sup>10-18,20-22</sup> However, the single-site DMFT cannot account for possible momentum-dependent correlation effects such as relative band shifts in opposite directions of, respectively, hole bands centered at  $\Gamma$  and electron bands centered at the Brillouin zone edge  $M$  (the so-called “blue/red shift”) in a large class of iron-based superconductors<sup>23-27</sup>, or the recently reported<sup>28</sup> possible momentum-dependent scattering rates in angular-resolved photoemission spectroscopy (ARPES) measurements of LiFeAs. Some of these effects have been suggested to play an important role in the superconducting pairing mechanism<sup>24,29-31</sup> as well.

Consideration of momentum dependence in the self-energy in real materials’ calculations are scarce but promising,<sup>32-38</sup> showing, for instance, effects of bandwidth widening and momentum-dependent bandshifts in the systems studied<sup>33,35,37</sup>. Here we explore this dependence by considering an approach where spin fluctuations play the dominant role and it allows both, a description

of local and non-local correlations on an equal footing.

The purpose of this work is twofold: (i) We first introduce the multi-orbital formulation of the Two-Particle Self-Consistent (TPSC) approach originally conceived for the single-orbital Hubbard model<sup>39</sup>, which provides momentum- and frequency- dependent self-energies in the intermediate coupling regime. (ii) We apply the method to the iron-based superconductor LiFeAs.

We find that the momentum-dependence obtained within the TPSC approach introduces drastic changes to the LiFeAs Fermi surface and bandstructure with respect to DFT results. First, the innermost hole pocket centered at  $\Gamma$  is shifted below the Fermi energy  $E_F$  as de Haas-van Alphen (dHvA) and ARPES<sup>26,40</sup> measurements already suggested. Second, we find a large accumulation of incoherent spectral weight around the  $\Gamma$  point as observed in ARPES<sup>24-26,28,30</sup>. Third, the relative “blue/red shift” of the bands centered at  $\Gamma$  and  $M$  respectively<sup>24,25</sup>, is properly described and, fourth, the momentum-averaged TPSC results agree with the results obtained from previous local DFT+DMFT calculations<sup>15,25</sup> pointing to an important relation between both approaches in this region of interactions.

**Models and methods.-** Starting from a DFT calculation of LiFeAs in the tetragonal crystal structure<sup>41</sup> within the Generalized Gradient Approximation (GGA)<sup>42</sup> using the full-potential linear augmented plane-wave basis from WIEN2K<sup>43</sup>, we derive an effective low-energy model comprizing the Fe  $3d$  orbitals using maximally localized Wannier functions as implemented in Wannier90<sup>44</sup> (see Supplemental Material<sup>45</sup>). We effectively then solve a 2-dimensional system by restricting our calculation to the  $k_z = 0$  plane, since the low-energy electronic structure shows only weak dispersion along  $k_z$ . In this Wannier-projected 2D model we have an electron occupation of 6. Interaction parameters for the lattice Hubbard model were obtained within the constrained random-phase approximation (cRPA)<sup>46</sup> on the DFT bandstructure (see Supplemental Material<sup>45</sup>).

The TPSC method considers the Luttinger-Ward functional  $\Phi[G]$ <sup>47,48</sup>, which is a functional of the interact-

\* zantout@itp.uni-frankfurt.de

ing Green's function  $G$  and yields the self-energy  $\Sigma$  and two-particle irreducible four-point vertex  $\Gamma$  as functional derivatives

$$\Sigma = \frac{\delta\Phi}{\delta G}, \quad \Gamma = \frac{\delta^2\Phi}{\delta G^2}. \quad (1)$$

Within the TPSC approach one approximates the vertex  $\Gamma$  to be static and momentum independent<sup>39</sup> (but fully orbital dependent). One obtains a set of self-consistent and conserving equations that satisfy the Pauli principle and Mermin-Wagner theorem. The range of validity of TPSC is the regime of weak to intermediate couplings where the local and static approximation of the vertex is valid, i.e. away from any phase transition. This method has been extended to multi-site,<sup>49–54</sup> nearest-neighbor interaction,<sup>55</sup> and multi-orbital<sup>56</sup> generalizations of the Hubbard model and has provided valuable insights on the pseudogap physics in the cuprates<sup>57</sup> and unconventional superconductivity.<sup>51,58,59</sup>

In the multi-orbital generalization of the TPSC method similar to the original formulation<sup>56</sup> we first introduce the non-interacting susceptibility  $\chi^0$  given by

$$\chi_{\lambda\mu\nu\xi}^0(\vec{q}, iq_m) = \left[ G_{\nu\lambda}^0 \star G_{\mu\xi}^0 \right] (\vec{q}, iq_m) \quad (2)$$

where  $G^0$  denotes the non-interacting Green's function in orbital-space,  $\star$  denotes a convolution over frequency and momentum and  $q_m = 2m\pi T$  the  $m$ -th bosonic Matsubara frequency. The interacting susceptibility  $\chi$  is decomposed into the spin and charge channel ( $\chi^{\text{sp}}$  and  $\chi^{\text{ch}}$  respectively) and reads

$$\begin{aligned} \chi^{\text{sp}}(\vec{q}, iq_m) &= [\mathbb{I} - \chi^0(\vec{q}, iq_m) U^{\text{sp}}]^{-1} 2\chi^0(\vec{q}, iq_m) \\ \chi^{\text{ch}}(\vec{q}, iq_m) &= [\mathbb{I} + \chi^0(\vec{q}, iq_m) U^{\text{ch}}]^{-1} 2\chi^0(\vec{q}, iq_m), \end{aligned} \quad (3)$$

where the inversion of a 4-index tensor is given as the matrix inverse after combining the first and last two indices of  $\lambda\mu\nu\xi$  into a superindex  $(\lambda\mu)(\nu\xi)$ .

We only consider the  $U_{\alpha\beta\beta}^{\text{ch/sp}}$  and  $U_{\alpha\beta\alpha\beta}^{\text{ch/sp}} = U_{\alpha\beta\beta\alpha}^{\text{ch/sp}}$  matrix elements of the renormalized irreducible vertices in the spin  $U^{\text{sp}}$  and the charge channel  $U^{\text{ch}}$  to be nonzero, corresponding to the atomic symmetry of 3d orbitals. Those elements are determined by enforcing the following local spin and charge sum rules

$$\begin{aligned} \frac{T}{N_{\vec{q}}} \sum_{\vec{q}, m} \chi_{\mu\nu\nu}^{\text{sp}}(\vec{q}, iq_m) &= \langle n_{\mu\uparrow} \rangle + \langle n_{\nu\uparrow} \rangle - 2\langle n_{\mu\uparrow} n_{\nu\downarrow} \rangle, \\ \frac{T}{N_{\vec{q}}} \sum_{\vec{q}, m} \chi_{\mu\mu\nu\nu}^{\text{sp}}(\vec{q}, iq_m) &\stackrel{\mu \neq \nu}{=} 2\langle n_{\mu\uparrow} n_{\nu\uparrow} \rangle - 2\langle n_{\mu\uparrow} n_{\nu\downarrow} \rangle, \\ \frac{T}{N_{\vec{q}}} \sum_{\vec{q}, m} \chi_{\mu\mu\nu\nu}^{\text{ch}}(\vec{q}, iq_m) &= 2\langle (n_{\mu\uparrow} + n_{\mu\downarrow}) n_{\nu\uparrow} \rangle - n_{\mu} n_{\nu}, \\ \frac{T}{N_{\vec{q}}} \sum_{\vec{q}, m} \chi_{\mu\nu\nu}^{\text{ch}}(\vec{q}, iq_m) &\stackrel{\mu \neq \nu}{=} \frac{n_{\mu} + n_{\nu}}{2} - \langle (4n_{\mu\uparrow} - 2n_{\mu\downarrow}) n_{\nu\uparrow} \rangle. \end{aligned} \quad (4)$$

In order to solve this underdetermined set of equations we employ an ansatz for the spin vertex  $U^{\text{sp}}$  that is motivated by the Kanamori-Brueckner screening<sup>39,56</sup> and introduce an additional particle-hole symmetrization to

keep all equations within TPSC particle-hole symmetric:

$$\begin{aligned} U_{\mu\mu\mu\mu}^{\text{sp}} &= \frac{1}{2} \left( \frac{\langle n_{\mu\uparrow} n_{\mu\downarrow} \rangle}{\langle n_{\mu\uparrow} \rangle \langle n_{\mu\downarrow} \rangle} + \text{particle} \leftrightarrow \text{hole} \right) U_{\mu\mu} \\ U_{\mu\nu\mu\nu}^{\text{sp}} &= \frac{1}{2} \left[ \frac{\langle n_{\mu\uparrow} n_{\mu\downarrow} \rangle}{\langle n_{\mu\uparrow} \rangle \langle n_{\mu\downarrow} \rangle} U_{\mu\nu} + \frac{\langle n_{\mu\uparrow} n_{\mu\downarrow} \rangle}{\langle n_{\mu\uparrow} \rangle \langle n_{\mu\downarrow} \rangle} (U_{\mu\nu} - J_{\mu\nu}) \right. \\ &\quad \left. + \text{particle} \leftrightarrow \text{hole} \right] = U_{\mu\mu\nu\nu}^{\text{sp}} = U_{\mu\nu\nu\mu}^{\text{sp}}. \end{aligned} \quad (5)$$

The local spin vertex  $U^{\text{sp}}$  can be obtained by iterating the equations above. For the charge channel we optimize  $U^{\text{ch}}$  in order to fulfill the corresponding charge sum rules, restricting to positive values of  $U^{\text{ch}}$  because in certain cases negative values can lead to non-causal self-energies. Due to the constraint we search for values of  $U^{\text{ch}}$  that minimize (see Supplemental Material<sup>45</sup>) the difference between left-hand side and right-hand side of the charge sum rules (Eq. (4)).

After the determination of the spin and charge vertices the self-energy  $\Sigma$  and interacting Green's function  $G$  are then given as

$$\Sigma_{\mu\nu} = \frac{1}{4} \sum_{\alpha, \beta} \underbrace{[U^{\text{sp}} \chi^{\text{sp}} U^{\text{sp},0} + U^{\text{ch}} \chi^{\text{ch}} U^{\text{ch},0}]_{\nu\alpha\mu\beta}}_{:=V_{\nu\alpha\mu\beta}} \star G_{\beta\alpha}^0$$

$$G(\vec{k}, i\omega_n) = \left[ (i\omega_n + \mu)\mathbb{I} - H_0(\vec{k}) - \Sigma(\vec{k}, i\omega_n) \right]^{-1}, \quad (6)$$

where the non-interacting vertices are zero except for the matrix elements:  $U_{\mu\mu\mu\mu}^{\text{sp/ch},0} = U_{\mu\mu}$ ,  $U_{\mu\mu\nu\nu}^{\text{ch},0} = 2U_{\mu\nu} - J_{\mu\nu}$  and  $U_{\mu\nu\mu\nu}^{\text{sp/ch},0} = U_{\mu\nu\nu\mu}^{\text{sp/ch},0} = U_{\mu\mu\nu\nu}^{\text{sp},0} = J_{\mu\nu}$  with  $\mu \neq \nu$ . No Hartree term is included in  $\Sigma$  since it is already contained in the DFT-derived Hamiltonian  $H_0$ .

Our multi-orbital extension of TPSC differs from previous formulations<sup>56</sup> on the following aspects: it restricts the self-consistent equations in the charge channel in Eq. (3) to ensure positivity of the spectral weight and chooses a symmetrized ansatz for  $U^{\text{sp}}$  (Eq. (5)). Furthermore, the set of local spin and charge sum rules (Eq. (4)) and bare vertex tensors  $U^{\text{ch},0}, U^{\text{sp},0}$  (Eq. (6)) and their dependence on  $U, J$  are derived from the Bethe-Salpeter equation for the self-energy  $\Sigma$  within TPSC<sup>39</sup>, which is different from the RPA derived expression of  $U^{\text{ch},0}, U^{\text{sp},0}$  only in the  $ijij$ -element,  $i \neq j$ .<sup>56</sup>

Our calculations were performed at  $T=0.015$  eV  $\approx 174$  K since this is the lowest accessible temperature before spin fluctuations get too strong and the TPSC approximation is not justified anymore. Nevertheless, we checked that the results presented below do not change in their trends up to room temperature (see Supplemental Material<sup>45</sup>).

**Results and discussion.** - In Fig. 1 we show the TPSC spectral function  $A(\vec{k}, \omega)$  for LiFeAs along  $\Gamma - X - M - \Gamma$  in the two-iron Brillouin zone. To emphasize the changes in the electronic structure beyond an overall bandwidth renormalization of about a factor of 2, we also plot the renormalized DFT bandstructure on top. We observe that the electronic correlations introduce a downshift of the hole states around the Fermi level at the  $\Gamma$ -point, while the electron states at  $M$  are slightly shifted up in

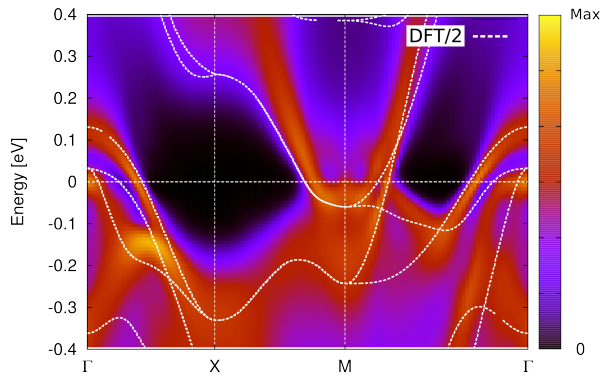


FIG. 1. Interacting spectral function  $A(\vec{k}, \omega)$  within the TPSC approach for LiFeAs in the two-iron Brillouin zone. For comparison we show the DFT(GGA) bandstructure renormalized by the average mass enhancement  $\approx 2$  (dotted lines). We observe an overall shrinking of the electron and hole pockets at  $\Gamma$  and  $M$  originating from the non-local components of the self-energy. The center hole pockets at  $\Gamma$  become incoherent and diffuse due to finite lifetime effects in the Fe  $3d_{xz}/3d_{yz}$  orbitals.

energy. The inner electron pocket being shifted by  $-0.1\text{eV}$  on average while the outer electron pocket is shifted by only  $-0.01\text{eV}$ . This leads to an overall shrinking of hole and electron pockets, corresponding to the “blue/red shift” seen in ARPES measurements<sup>24,26</sup> compared to the DFT bandstructure. Apart from orbital dependence the shrinkings are momentum-dependent. For example, along  $\Gamma - X$  the middle hole pocket shrinks to approximately 20% of its size compared to the renormalized DFT bandstructure while all other parts of the Fermi surface shrink to 80-90% of their original size. The inner hole pocket at  $\Gamma$ , composed of Fe  $3d_{xz}/3d_{yz}$  orbital character (see Fig. 2 (a)), becomes very diffuse at the Fermi level due to incoherent scattering processes, leading to a significant reduction of the lifetime of quasi-particle excitations. This manifests in a broad Fermi surface feature very similar to the one observed in ARPES<sup>24-26,28,30</sup>. The maximum of the spectral function of the two inner hole pockets at  $\Gamma$  is shifted basically on top of the Fermi level but retains significant spectral weight at higher and lower binding energies - the shift being on average  $0.18\text{eV}$  for both while for the outer hole pocket it is  $0.1\text{eV}$ . We expect that the inclusion of spin-orbit coupling, which is beyond our current approach, will split this feature, effectively pushing one hole band below and the other above the Fermi level, giving rise to only one central hole Fermi surface pocket, which would be in very good agreement with previous ARPES data<sup>26,60</sup> as well as de Haas-van Alphen (dHvA) experiments.<sup>40</sup>

We can trace back these Fermi surface modifications to the value of the self-energy at the specific  $\vec{k}$ -points in the Brillouin zone: The largest contribution to the diagonal elements of the self-energy in Eq. (6) stems from  $V_{abab}$ , which is peaked at  $\vec{k} = \{(\pm\pi, 0), (0, \pm\pi)\}$ . Following the argumentation of Ref. 23, this leads to a negative (posi-

tive) real part of the self-energy in the vicinity of the hole (electron) pockets and thus to the observed “blue/red shift” and therefore it is a consequence of non-local spin fluctuations.

In Fig. 2 we show the orbitally-resolved Fermi surface obtained from DFT (within GGA) (Fig. 2 (a)), DFT+TPSC (Fig. 2 (b)) and DFT+“local TPSC” where the momentum dependent TPSC self-energy  $\Sigma(\vec{k}, \omega)$  has been approximated by its local component  $\frac{1}{N_k} \sum_{\vec{k}} \Sigma(\vec{k}, \omega)$  (Fig. 2 (c)). The DFT Fermi surface reveals three well-defined distinct hole pockets centered at  $\Gamma$  with circular to square shape and two electron pockets centered at  $M$ . As can already be deduced from the spectral function  $A(\vec{k}, \omega)$  in Fig. 1, the Fermi surface experiences appreciable changes due to the TPSC self-energy contributions. All pockets are reduced in size, with the remaining spectral weight of the two center hole pockets of Fe  $3d_{xz}/3d_{yz}$  character at  $\Gamma$  becoming incoherent and forming a flower-like shape, while the outer hole pocket of  $3d_{xy}$  character stays coherent as confirmed in ARPES measurements<sup>24,26</sup>. The electron pockets at  $M$  shrink slightly and broaden, since they are mostly composed of the most incoherent  $3d_{xz}/3d_{yz}$  as well.

The observed shrinking of the hole and electron pockets deviates significantly from published DFT+DMFT results, most likely due to the inclusion of non-local correlations in the TPSC approach which go beyond the DMFT approximation where the self-energy is purely local. In order to confirm this assumption we separate the local from the non-local correlation effects by employing a DMFT-like approximation on the TPSC self-energy. We approximate the full momentum-dependent TPSC self-energy  $\Sigma(\vec{k}, \omega)$  by its local component and compare the resulting Fermi surface to the full result in Fig. 2 (c). The so obtained Fermi surface indeed recovers the result obtained within published DFT+DMFT<sup>15,25</sup>, and, when considering the DFT+DMFT results for the same model as used in this work (see Supplemental Material<sup>45</sup>), the agreement is almost perfect (compare Fig. 2 (c) and (d)). DFT+DMFT calculations with a different double counting scheme<sup>22</sup> see a more pronounced - although coherent- flower-like shape of spectral weight around  $\Gamma$  but don’t account for the “blue/red shift”. This shows that when taking into account non-local fluctuations, the local Coulomb interaction gives rise to a significant momentum-dependent self-energy and can account for the experimentally observed “blue/red shift”. Interestingly, within the local approximation (local TPSC) the center hole pockets at  $\Gamma$  become again coherent, which is also in correspondence with the DMFT result. This shows that the quasi-particle scattering rate itself is strongly momentum and orbital dependent, which has in fact been observed in recent ARPES experiments<sup>26,28</sup>, where the inner  $3d_{xz}/3d_{yz}$  derived hole Fermi surface have been found to be incoherent while the outer  $3d_{xy}$  hole pocket shows Fermi liquid behavior.

Since Fermi-liquid theory predicts a quadratic energy

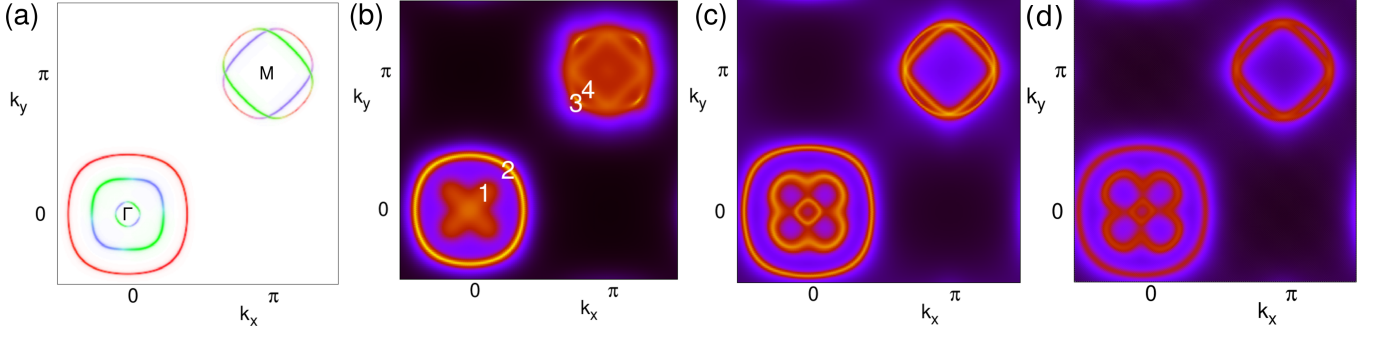


FIG. 2. (a) Orbital-resolved Fermi surface obtained from DFT(GGA) where the dominant orbital characters are  $d_{xy}$  (red),  $d_{yz}$  (blue) and  $d_{xz}$  (green). Three hole pockets are centered around  $\Gamma$  and two electron pockets around the  $M$  point. (b) Fermi surface from DFT+TPSC. We observe strong incoherence effects on the inner hole and electron pockets. The two inner hole pockets become very incoherent and form a flower-like shaped region of spectral weight. (c) Fermi surface from DFT+"local TPSC" where the momentum dependent TPSC self-energy  $\Sigma(\vec{k}, \omega)$  has been approximated by its local component  $\frac{1}{N_{\vec{k}}} \sum_{\vec{k}} \Sigma(\vec{k}, \omega)$ . In this approximation the Fermi surface recovers well published DFT+DMFT result<sup>15,25</sup>. (d) DFT+DMFT Fermi surface for the same model (see Supplemental Material<sup>45</sup>) as used in this work. We see a strong similarity to the DFT+"local TPSC" result in (c).

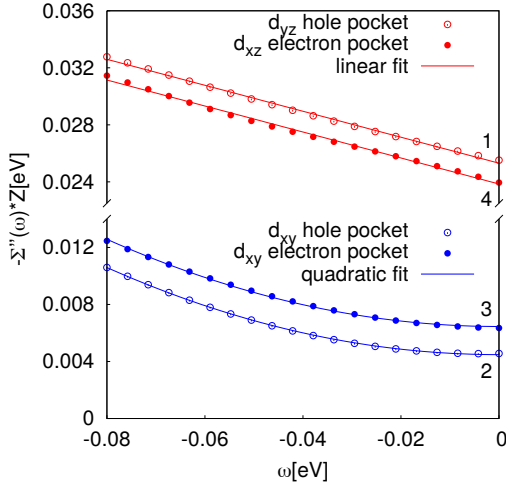


FIG. 3. Quasi-particle lifetimes  $-Z_{\vec{k}} \Sigma''(\vec{k}, \omega)$  along  $\Gamma - M$  as a function of the binding energy  $\omega$  (numbers on the right correspond to positions in Fig.2(c)). We find that the quasi-particles with  $d_{xz/yz}$  character display a linear dependence in  $\omega$  while the electron pockets have a quadratic increase with energy. (See Supplemental Material<sup>45</sup>)

dependence of quasi-particles' lifetimes near the Fermi energy, deviations from this energy dependence are also a signature for non-Fermi liquid behavior. It is therefore compelling to analyze the energy dependencies of the scattering rate within the TPSC approach. For this, we present the quasi-particle lifetime  $-Z_{\vec{k}} \Sigma''(\vec{k}, \omega)$  with

$$Z_{\vec{k}} = \frac{1}{1 - \left. \frac{\partial \Sigma''(\vec{k}, i\omega_n)}{\partial \omega_n} \right|_{i\omega_n \rightarrow 0^+}} \quad (7)$$

in Fig. 3 at four different  $\vec{k}$ -points in momentum space

following the  $\Gamma - M$  path. Along this path the dominating contributions are (1)  $d_{yz}$  hole pocket, (2)  $d_{xy}$  hole pocket, (3)  $d_{xy}$  electron pocket and (4)  $d_{xz}$  electron pocket (see Fig. 2(a) and (b)). The energy dependence of the quasi-particle lifetimes for the  $d_{xz/yz}$  electron and hole pockets (red symbols in Fig. 3) are in good agreement with the results of Ref. 26 with values between 0.025eV and 0.035eV. The energy dependence shows a very shallow linear behavior (fitted slopes are of the order of  $10^{-3}$ , see Supplemental Material<sup>45</sup>) similar to the measurements from Ref. 26. The quasi-particle lifetimes of the  $d_{xy}$  hole and electron pockets (blue symbols in Fig. 3), in contrast, show at the considered  $k$ -points a quadratic increase in energy as in the ARPES measurements of Ref. 26, suggesting a Fermi-liquid-like behavior. Although our data was obtained at  $T \approx 174K$  in contrast to the  $T = 25K$  in Ref. 26, we are confident that our results are still valid at low temperatures, since for example in  $\text{Ba}(\text{Fe}_{0.92}\text{Co}_{0.08})_2\text{As}_2$  it has been found that the quasi-particle lifetimes for the hole  $d_{xz/yz}$  orbitals showed weak temperature dependence. We also checked how these results depend on the  $\vec{k}$ -path and found that small translations along the tip of electron pocket (3) reveal a linear dependence of the quasi-particle lifetime as can already be expected since the quasi-particle weight gets incoherent away from the point (3) (see Fig. 2(b)).

*Summary.* - In conclusion, we presented a multi-orbital TPSC scheme that respects local spin and charge sum rules. This method includes effects of local and non-local correlations on an equal footing within the validity of the local approximation of the irreducible 4-point vertex and thus yields momentum- and frequency-dependent self-energies. We applied this method to the multi-orbital iron-based superconductor  $\text{LiFeAs}$  and found that the non-local components of the self-energy are decisive to explain its experimentally observed spectral function

$A(k, \omega)$  and Fermi surface. Taking into account non-local correlations we observe a “blue/red shift” of the electronic structure, where the hole bands at the Brillouin zone center are lowered in energy, while the electron bands in the corner of the Brillouin zone are slightly shifted upwards, resulting in an overall reduction of the size of the Fermi surface pockets. Overall we find very good agreement with ARPES and dHvA experiments, where the “blue/red shift” was first observed. We could show that our TPSC approach within a local approximation to the self-energy recovers the DFT+DMFT result which does not exhibit the “blue/red shift”, both benchmarking the TPSC result and showing the importance of going beyond the local picture of DMFT in order to understand the electronic structure of iron-based superconductors. Furthermore, we also found a strong momentum

and non-quadratic energy dependence of the electronic scattering rate, in good agreement with recent ARPES measurements.

## ACKNOWLEDGMENTS

This work was supported by the German Research Foundation (Deutsche Forschungsgemeinschaft) under grant SFB/TR 49. We would like to thank S. Bhattacharyya, S. Borisenko, V. Borisov, J. Fink, P.J. Hirschfeld, G. Kotliar and Y. Li for discussions. R. V. acknowledges the KITP for hospitality where aspects of this work were discussed. The research at KITP was supported in part by NSF Grant No. NSF PHY-1748958.

- 
- <sup>1</sup> Y. Kamihara, T. Watanabe, M. Hirano, and H. Hosono, *Journal of the American Chemical Society* **130**, 3296 (2008).
  - <sup>2</sup> M. Rotter, M. Tegel, and D. Johrendt, *Phys. Rev. Lett.* **101**, 107006 (2008).
  - <sup>3</sup> S. Lebegue, *Phys. Rev. B* **75**, 035110 (2007).
  - <sup>4</sup> D. J. Singh and M.-H. Du, *Phys. Rev. Lett.* **100**, 237003 (2008).
  - <sup>5</sup> I. I. Mazin, M. D. Johannes, L. Boeri, K. Koepernik, and D. J. Singh, *Phys. Rev. B* **78**, 085104 (2008).
  - <sup>6</sup> C. Cao, P. J. Hirschfeld, and H.-P. Cheng, *Phys. Rev. B* **77**, 220506(R) (2008).
  - <sup>7</sup> Q. Si and E. Abrahams, *Phys. Rev. Lett.* **101**, 076401 (2008).
  - <sup>8</sup> M. M. Qazilbash, J. J. Hamlin, R. E. Baumbach, L. Zhang, D. J. Singh, M. B. Maple, and D. N. Basov, *Nature Physics* **5**, 647 (2009).
  - <sup>9</sup> F. Rullier-Albenque, D. Colson, A. Forget, and H. Alloul, *Phys. Rev. Lett.* **103**, 057001 (2009).
  - <sup>10</sup> K. Haule and G. Kotliar, *New Journal of Physics* **11**, 025021 (2009).
  - <sup>11</sup> L. de’ Medici, S. R. Hassan, M. Capone, and X. Dai, *Phys. Rev. Lett.* **102**, 126401 (2009).
  - <sup>12</sup> M. Aichhorn, S. Biermann, T. Miyake, A. Georges, and M. Imada, *Phys. Rev. B* **82**, 064504 (2010).
  - <sup>13</sup> P. Hansmann, R. Arita, A. Toschi, S. Sakai, G. Sangiovanni, and K. Held, *Phys. Rev. Lett.* **104**, 197002 (2010).
  - <sup>14</sup> Z. P. Yin, K. Haule, and G. Kotliar, *Nature Materials* **10**, 932 (2011).
  - <sup>15</sup> J. Ferber, K. Foyevtsova, R. Valentí, and H. O. Jeschke, *Phys. Rev. B* **85**, 094505 (2012).
  - <sup>16</sup> P. Werner, M. Casula, T. Miyake, F. Aryasetiawan, A. J. Millis, and S. Biermann, *Nature Physics* **8**, 331 (2012).
  - <sup>17</sup> J. Ferber, H. O. Jeschke, and R. Valentí, *Phys. Rev. Lett.* **109**, 236403 (2012).
  - <sup>18</sup> D. V. Evtushinsky, M. Aichhorn, Y. Sassa, Z.-H. Liu, J. Maletz, T. Wolf, A. N. Yaresko, S. Biermann, S. V. Borisenko, and B. Büchner, *arXiv preprint arXiv:1612.02313* (2016).
  - <sup>19</sup> E. Bascones, B. Valenzuela, and M. J. Calderón, *Comptes Rendus Physique* **17**, 36 (2016).
  - <sup>20</sup> M. D. Watson, S. Backes, A. A. Haghighirad, M. Hoesch, T. K. Kim, A. I. Coldea, and R. Valentí, *Phys. Rev. B* **95**, 081106(R) (2017).
  - <sup>21</sup> H. Miao, Z. P. Yin, S. F. Wu, J. M. Li, J. Ma, B.-Q. Lv, X. P. Wang, T. Qian, P. Richard, L.-Y. Xing, X.-C. Wang, C. Q. Jin, K. Haule, G. Kotliar, and H. Ding, *Phys. Rev. B* **94**, 201109(R) (2016).
  - <sup>22</sup> R. Nourafkan, G. Kotliar, and A.-M. S. Tremblay, *Phys. Rev. Lett.* **117**, 137001 (2016).
  - <sup>23</sup> L. Ortenzi, E. Cappelluti, L. Benfatto, and L. Pietronero, *Phys. Rev. Lett.* **103**, 046404 (2009).
  - <sup>24</sup> S. V. Borisenko, V. B. Zabolotnyy, D. V. Evtushinsky, T. K. Kim, I. V. Morozov, A. N. Yaresko, A. A. Kordyuk, G. Behr, A. Vasiliev, R. Follath, and B. Büchner, *Phys. Rev. Lett.* **105**, 067002 (2010).
  - <sup>25</sup> G. Lee, H. S. Ji, Y. Kim, C. Kim, K. Haule, G. Kotliar, B. Lee, S. Khim, K. H. Kim, K. S. Kim, K.-S. Kim, and J. H. Shim, *Phys. Rev. Lett.* **109**, 177001 (2012).
  - <sup>26</sup> V. Brouet, D. LeBoeuf, P.-H. Lin, J. Mansart, A. Taleb-Ibrahimi, P. Le Fèvre, F. Bertran, A. Forget, and D. Colson, *Phys. Rev. B* **93**, 085137 (2016).
  - <sup>27</sup> Y. S. Kushnirenko, A. A. Kordyuk, A. V. Fedorov, E. Haubold, T. Wolf, B. Büchner, and S. V. Borisenko, *Phys. Rev. B* **96**, 100504(R) (2017).
  - <sup>28</sup> J. Fink, J. Nayak, E. D. L. Rienks, J. Bannies, S. Wurmehl, S. Aswartham, I. Morozov, R. Kappenberger, M. A. ElGhazali, L. Craco, H. Rosner, C. Felser, and B. Büchner, *Phys. Rev. B* **99**, 245156 (2019).
  - <sup>29</sup> Y. Wang, A. Kreisel, V. B. Zabolotnyy, S. V. Borisenko, B. Büchner, T. A. Maier, P. J. Hirschfeld, and D. J. Scalapino, *Phys. Rev. B* **88**, 174516 (2013).
  - <sup>30</sup> H. Miao, T. Qian, X. Shi, P. Richard, T. K. Kim, M. Hoesch, L. Y. Xing, X.-C. Wang, C.-Q. Jin, J.-P. Hu, and H. Ding, *Nature communications* **6**, 6056 (2015).
  - <sup>31</sup> D. Altenfeld, P. J. Hirschfeld, I. I. Mazin, and I. Eremin, *Phys. Rev. B* **97**, 054519 (2018).
  - <sup>32</sup> S. Biermann, F. Aryasetiawan, and A. Georges, *Phys. Rev. Lett.* **90**, 086402 (2003).
  - <sup>33</sup> J. M. Tomczak, M. van Schilfhaarde, and G. Kotliar, *Phys. Rev. Lett.* **109**, 237010 (2012).
  - <sup>34</sup> J. M. Tomczak, M. Casula, T. Miyake, and S. Biermann, *Phys. Rev. B* **90**, 165138 (2014).
  - <sup>35</sup> A. van Roekeghem, T. Ayral, J. M. Tomczak, M. Casula,

- N. Xu, H. Ding, M. Ferrero, O. Parcollet, H. Jiang, and S. Biermann, *Phys. Rev. Lett.* **113**, 266403 (2014).
- <sup>36</sup> S. Biermann, *J. Phys.: Condens. Matter* **26**, 173202 (2014).
- <sup>37</sup> S. Li, N. Kaushal, Y. Wang, Y. Tang, G. Alvarez, A. Nocera, T. A. Maier, E. Dagotto, and S. Johnston, *Phys. Rev. B* **94**, 235126 (2016).
- <sup>38</sup> P. Sémon, K. Haule, and G. Kotliar, *Phys. Rev. B* **95**, 195115 (2017).
- <sup>39</sup> Y.M. Vilk and A.-M.S. Tremblay, *J. Phys. I France* **7**, 1309 (1997).
- <sup>40</sup> C. Putzke, A. I. Coldea, I. Guillaumon, D. Vignolles, A. McCollam, D. LeBoeuf, M. D. Watson, I. I. Mazin, S. Kasahara, T. Terashima, T. Shibauchi, Y. Matsuda, and A. Carrington, *Phys. Rev. Lett.* **108**, 047002 (2012).
- <sup>41</sup> I. Morozov, A. Boltalin, O. Volkova, A. Vasiliev, O. Kataeva, U. Stockert, M. Abdel-Hafiez, D. Bombor, A. Bachmann, L. Harnagea, M. Fuchs, H.-J. Grafe, G. Behr, R. Klingeler, S. Borisenko, C. Hess, S. Wurmehl, and B. Büchner, *Crystal Growth & Design* **10**, 4428 (2010).
- <sup>42</sup> J. P. Perdew, K. Burke, and M. Ernzerhof, *Phys. Rev. Lett.* **77**, 3865 (1996).
- <sup>43</sup> P. Blaha, K. Schwarz, G. K. H. Madsen, D. Kvasnicka, and J. Luitz, Vienna University of Technology, Vienna (2001).
- <sup>44</sup> A. A. Mostofi, J. R. Yates, G. Pizzi, Y.-S. Lee, I. Souza, D. Vanderbilt, and N. Marzari, *Computer Physics Communications* **185**, 2309 (2014).
- <sup>45</sup> See Supplemental Material at [url] for further information on the model, numerical details, the temperature dependence and the comparison to DMFT, which includes Refs. 15, 21, 25, 39, 43, 44, 61–63.
- <sup>46</sup> H. Jiang, R. I. Gómez-Abal, X.-Z. Li, C. Meisenbichler, C. Ambrosch-Draxl, , and M. Scheffler, *Computer Phys. Commun.* **184**, 348 (2012).
- <sup>47</sup> P. C. Martin and J. Schwinger, *Phys. Rev.* **115**, 1342 (1959).
- <sup>48</sup> G. Baym, *Phys. Rev.* **127**, 1391 (1962).
- <sup>49</sup> S. Arya, P. V. Sriluckshmy, S. R. Hassan, and A.-M. S. Tremblay, *Phys. Rev. B* **92**, 045111 (2015).
- <sup>50</sup> H. Aizawa, K. Kuroki, and J.-i. Yamada, *Phys. Rev. B* **92**, 155108 (2015).
- <sup>51</sup> K. Zantout, M. Altmeyer, S. Backes, and R. Valentí, *Phys. Rev. B* **97**, 014530 (2018).
- <sup>52</sup> T. Mertz, K. Zantout, and R. Valentí, *Phys. Rev. B* **98**, 235105 (2018).
- <sup>53</sup> H. Aizawa and K. Kuroki, *Phys. Rev. B* **97**, 104507 (2018).
- <sup>54</sup> K. Nishiguchi, S. Teranishi, K. Kusakabe, and H. Aoki, *Phys. Rev. B* **98**, 174508 (2018).
- <sup>55</sup> B. Davoudi and A.-M. S. Tremblay, *Phys. Rev. B* **74**, 035113 (2006).
- <sup>56</sup> H. Miyahara, R. Arita, and H. Ikeda, *Phys. Rev. B* **87**, 045113 (2013).
- <sup>57</sup> A.-M. S. Tremblay, “Two-particle-self-consistent approach for the hubbard model,” in *Strongly Correlated Systems: Theoretical Methods*, edited by A. Avella and F. Mancini (Springer-Verlag Berlin Heidelberg, 2012) pp. 409–453.
- <sup>58</sup> B. Kyung, J.-S. Landry, and A.-M. S. Tremblay, *Phys. Rev. B* **68**, 174502 (2003).
- <sup>59</sup> D. Ogura and K. Kuroki, *Phys. Rev. B* **92**, 144511 (2015).
- <sup>60</sup> Y. S. Kushnirenko, D. V. Evtushinsky, T. K. Kim, I. V. Morozov, S. Wurmehl, S. Aswartham, A. V. Chubukov, and S. V. Borisenko, arXiv preprint arXiv:1810.04446 (2018).
- <sup>61</sup> T. Miyake, K. Nakamura, R. Arita, and M. Imada, *Journal of the Physical Society of Japan* **79**, 044705 (2010), <https://doi.org/10.1143/JPSJ.79.044705>.
- <sup>62</sup> R. Levy, J. LeBlanc, and E. Gull, *Computer Physics Communications* **215**, 149 (2017).
- <sup>63</sup> A. Gaenko, A. Antipov, G. Carcassi, T. Chen, X. Chen, Q. Dong, L. Gamper, J. Gukelberger, R. Igarashi, S. Iskakov, M. Knz, J. LeBlanc, R. Levy, P. Ma, J. Paki, H. Shinaoka, S. Todo, M. Troyer, and E. Gull, *Computer Physics Communications* **213**, 235 (2017).

# Supplemental Material: Effect of non-local correlations on the electronic structure of LiFeAs

Karim Zantout,<sup>1</sup> Steffen Backes,<sup>2</sup> and Roser Valentí<sup>1</sup>

<sup>1</sup>*Institut für Theoretische Physik, Goethe-Universität Frankfurt, 60438 Frankfurt am Main, Germany*

<sup>2</sup>*CPHT, CNRS, Institut Polytechnique de Paris, F-91128 Palaiseau, France*

## I. LOW-ENERGY MODEL

Our DFT-derived low-energy Hamiltonian is given by

$$\begin{aligned} H = & \underbrace{\sum_{\alpha,\beta,i,j,\sigma} (t_{ij,\alpha\beta} - \mu\delta_{i,j}\delta_{\alpha,\beta}) c_{i\alpha\sigma}^\dagger c_{j\beta\sigma}}_{:=H_0} \\ & + \sum_{\alpha,\beta,i,\sigma} \frac{U_{\alpha\beta}}{2} n_{i\alpha\sigma} n_{i\beta-\sigma} + \sum_{\substack{\alpha,\beta,i,\sigma \\ \alpha \neq \beta}} \frac{U_{\alpha\beta} - J_{\alpha\beta}}{2} n_{i\alpha\sigma} n_{i\beta\sigma} \\ & - \sum_{\substack{\alpha,\beta,i,\sigma \\ \alpha \neq \beta}} \frac{J_{\alpha\beta}}{2} \left( c_{i\alpha\sigma}^\dagger c_{i\alpha-\sigma} c_{i\beta-\sigma}^\dagger c_{i\beta\sigma} + c_{i\alpha\sigma}^\dagger c_{i\beta-\sigma} c_{i\alpha-\sigma}^\dagger c_{i\beta\sigma} \right), \end{aligned}$$

where  $t_{ij,\alpha\beta}$  denote the hopping parameters from orbital  $\alpha$  in unit cell  $i$  to orbital  $\beta$  in unit cell  $j$ ,  $\mu$  is the chemical potential,  $c_{i\alpha\sigma}^\dagger$  ( $c_{i\alpha\sigma}$ ) creates (annihilates) an electron in unit cell  $i$  at orbital  $\alpha$  with spin  $\sigma$ . The Hamiltonian is constructed in the basis of the Fe 3d orbitals using maximally localized Wannier functions as implemented in Wannier90<sup>44</sup>.

## II. INTERACTION PARAMETERS

The interaction parameters obtained from cRPA are given as (in the  $d_{z^2}$ ,  $d_{x^2-y^2}$ ,  $d_{xy}$ ,  $d_{xz}$ ,  $d_{yz}$  basis of the Fe 3d orbitals)

$$U = \begin{pmatrix} 3.40 & 1.94 & 2.03 & 2.39 & 2.39 \\ 1.94 & 2.54 & 2.13 & 1.89 & 1.89 \\ 2.03 & 2.13 & 2.66 & 1.98 & 1.98 \\ 2.39 & 1.89 & 1.98 & 2.75 & 2.02 \\ 2.39 & 1.89 & 1.98 & 2.02 & 2.75 \end{pmatrix} \text{ eV}$$

and

$$J = \begin{pmatrix} 0 & 0.49 & 0.51 & 0.34 & 0.34 \\ 0.49 & 0 & 0.23 & 0.39 & 0.39 \\ 0.51 & 0.23 & 0 & 0.41 & 0.41 \\ 0.34 & 0.39 & 0.41 & 0 & 0.41 \\ 0.34 & 0.39 & 0.41 & 0.41 & 0 \end{pmatrix} \text{ eV.} \quad (1)$$

We employed a  $d-d$  model, i.e. the same Wannier basis was used for the Hamiltonian and the screening of only the Fe 3d orbitals has been removed. A  $k$ -mesh of  $8 \times 8 \times 5$  was used for the integration over the Brillouin zone.

Compared to previously published interaction values of LiFeAs obtained from cRPA<sup>61</sup> we observe smaller values of  $U_{d_{xy}, d_{xy}} = 2.66 \text{ eV}$  instead of  $3.51 \text{ eV}$  or  $U_{d_{xz}, d_{xz}} = U_{d_{yz}, d_{yz}} = 2.75 \text{ eV}$  instead of  $3.16 \text{ eV}$ . We attribute the differences to the following points:

1) In Ref. 61 the DFT calculation has been performed using the full-potential LMTO basis, while we have used the full-potential LAPW basis from Wien2K<sup>43</sup>.

2) We found that the cRPA calculation is sensitive to the resolution of the discretization in momentum space and a fine grid is needed for proper convergence. In our calculation we employed an  $8 \times 8 \times 5$   $k$ -mesh, while the reference used a smaller mesh of  $4 \times 4 \times 4$ . We checked the dependence on the  $k$ -mesh by performing the calculation with the smaller meshes and found a significant difference in the spread of the Wannier functions:

	Spread of $d_{z^2}$	$d_{x^2-y^2}$	$d_{xy}$	$d_{xz/yz}$
4x4x4 $k$ -points	$2.85 \text{ \AA}^2$	$3.53 \text{ \AA}^2$	$2.85 \text{ \AA}^2$	$3.09 \text{ \AA}^2$
8x8x5 $k$ -points	$2.91 \text{ \AA}^2$	$8.74 \text{ \AA}^2$	$3.84 \text{ \AA}^2$	$3.91 \text{ \AA}^2$

The spread increases significantly for a denser  $k$ -mesh, explaining why we find lower interaction values with an  $8 \times 8 \times 5$   $k$ -mesh compared to the  $4 \times 4 \times 4$  mesh used in Ref. 61. We also performed the cRPA calculation for  $4 \times 4 \times 4$   $k$ -meshes and obtained larger interaction values that are closer to the one shown in the reference:  $U_{d_{xy}, d_{xy}} = 3.03 \text{ eV}$  or  $U_{d_{xz}, d_{xz}} = U_{d_{yz}, d_{yz}} = 2.8 \text{ eV}$ . We think our results are sufficiently converged since the values changed only about 5-10% when increasing the mesh from  $7 \times 7 \times 5$  to  $8 \times 8 \times 5$   $k$ -points. A finer calculation with a  $9 \times 9 \times 6$   $k$ -mesh could not be done due to memory constraints.

## III. COMPUTATIONAL DETAILS

For the momentum-space integration we employed an adaptive cubature method based on a three-point formula for triangles with an integration tolerance of  $10^{-6}$  to evaluate the non-interacting susceptibility. We obtained all quantities on a  $100 \times 100$   $\vec{k}$ -grid in order to account for any singular features. The fast Fourier transformation and the circular convolution theorem was used for an efficient implementation of Eq. 6 in the main document. The summation over fermionic Matsubara frequencies was performed for  $N_{\text{Mats}} = 250 \cdot (0.025/T) \text{ eV}$  points and for bosonic Matsubara frequencies we took  $2N_{\text{Mats}}/3$  points. In both cases we included high-frequency corrections up to the order of  $\frac{1}{\omega^2}$  by extrapolation of the high-frequency tail. The calculations were performed at  $T = 0.015 \text{ eV} \approx 174 \text{ K}$ . Analytical continuation was performed with the maximum entropy Code from<sup>62</sup> in the case of the spectral function  $A(\vec{k}, \omega)$  and with Padé approximation for the imaginary part of the self-energy  $\Sigma''(\vec{k}, \omega)$  and calculated  $Z_{\vec{k}}$  via linear extrapolation  $i\omega \rightarrow 0$  in the case of quasi-particle lifetimes.

During the optimization procedure of  $U^{ch}$  we encounter deviations of at most 6% between left-hand and right-hand side of the charge sum rules (Eq. 4 in the main document) in our calculations of LiFeAs. Since the charge channel has a much smaller contribution to the self-energy  $\Sigma$  compared to the spin channel we can estimate the effect of this inaccuracy on our results to be negligible.



The fitting curves  $\tau$  for the quasi-particle lifetimes  $-Z_{\vec{k}}\Sigma''(\vec{k},\omega)$  from Fig. 3 are given by

$$\begin{aligned} d_{yz} \text{ hole pocket: } \tau(\omega) &= 25\text{meV} - 0.09\omega \\ d_{xz} \text{ electron pocket: } \tau(\omega) &= 24\text{meV} - 0.091\omega \\ d_{xy} \text{ hole pocket: } \tau(\omega) &= 4.5\text{meV} + \frac{0.95}{\text{eV}}\omega^2 \\ d_{xz} \text{ electron pocket: } \tau(\omega) &= 6.5\text{meV} + \frac{0.96}{\text{eV}}\omega^2. \end{aligned}$$

#### IV. TEMPERATURE DEPENDENCE

In the range of temperatures studied which is  $T \gtrsim 175\text{K}$  we see that the trends in the results stay the same, for instance the Fermi surface keeps its topology (Fig. 4). We also see that the quasi-particle lifetime  $-Z_{\vec{k}}\Sigma''(\vec{k},\omega=0)$

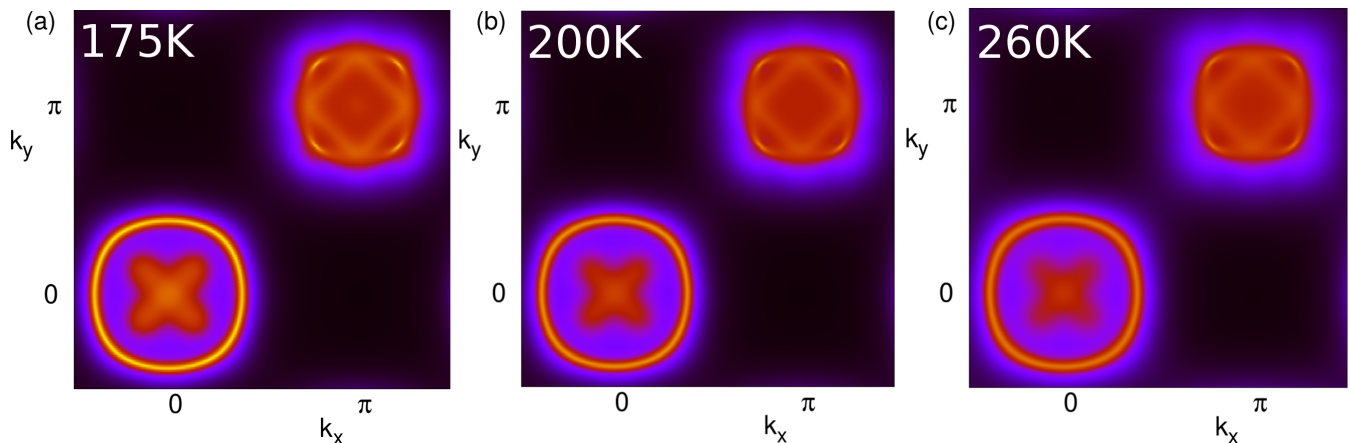


FIG. 1. DFT+TPSC Fermi surfaces at (a)  $T = 175\text{ K}$ , (b)  $T = 200\text{ K}$  and (c)  $T = 260\text{ K}$ . We see that the Fermi surface changes only marginally due to thermal decoherence.

at the  $d_{xy}$  hole pocket seems to show a linear increase (see Fig. 5) in accordance with the coherence-incoherence crossover region measured in Ref. 21.

#### V. LOCAL TPSC AND DMFT

We performed a local approximation to the TPSC self-energy and found that it recovers the published DMFT result<sup>15,25</sup>. This means the Fermi surface is almost identical to the DFT Fermi surface except for subtle changes in the middle hole pocket around  $\Gamma$ . This shows that the TPSC approximation is able to access the local correlations in LiFeAs in the same extent as DMFT employing a numerically exact impurity solver. Since our model involves additional approximations discussed in the main manuscript (two-dimensional lattice using a one iron unit cell) we performed an additional standard DMFT calculation with the same noninteracting Hamiltonian and identical parameters used in the TPSC calculation. For the solution of the impurity model we used the continuous-time Quantum Monte-Carlo Solver in the segment picture as implemented in the ALPSCore package<sup>44,63</sup>.

In Fig.6 we show a comparison between the low-energy momentum-resolved spectral function obtained from the local TPSC and the DMFT calculation, compared to the renormalized DFT result. Both cases basically reproduce the DFT electronic structure at the Fermi level except for an overall bandwidth renormalization, which is slightly stronger in DMFT (factor 2.1) than in local-TPSC (factor 2), and stronger degree of broadening at higher energies. There is an additional small modification of the middle hole pocket along  $\Gamma - M$  in DMFT, which is not captured in local TPSC. The fact that both approaches agree very well and very closely reproduce the DFT electronic structure, most importantly not exhibiting an overall shrinking of Fermisurface pockets with a blue/red shift, shows that TPSC is able to capture the local electronic correlations and that non-local extensions are needed to explain the electronic structure of LiFeAs.

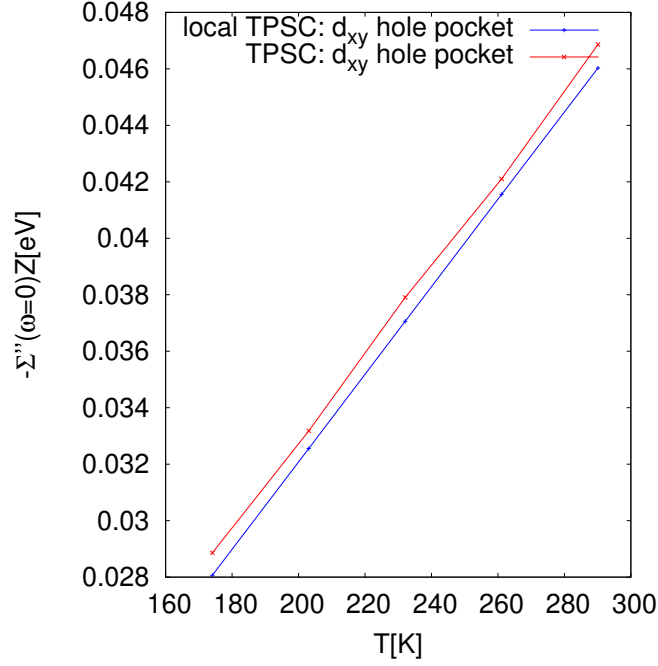


FIG. 2. Quasi-particle lifetime at the  $d_{xy}$  hole pocket within DFT+TPSC and DFT+“local” TPSC. We see a linear increase in both due to thermal decoherence and a weak momentum-dependence.

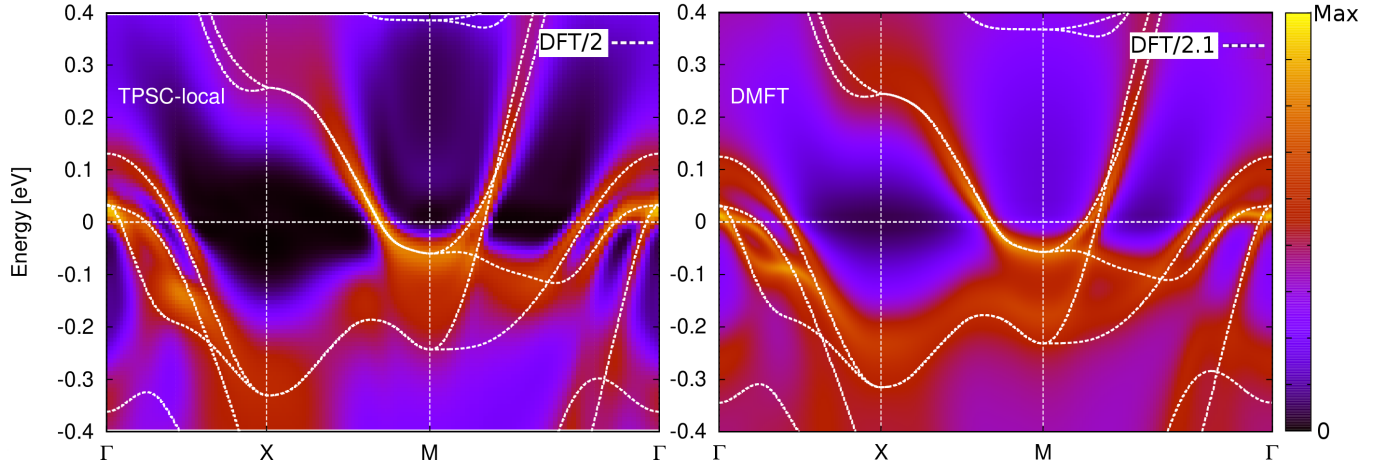


FIG. 3. Left: The momentum-resolved spectral function of LiFeAs within the local TPSC approximation (see main text). Right: DMFT The momentum-resolved spectral function using the same noninteracting Hamiltonian and parameters as in the TPSC calculation.

To quantitatively compare the two approaches, we plot a comparison of the local TPSC self-energy and the DMFT impurity self-energy in Fig.7. We observe a good agreement between the two approaches, especially in the low-energy part of the imaginary part of the self-energy. This part is the relevant one for the low-energy electronic states like the Fermi surface. A noticeable difference is the stronger renormalization of about a factor of 2.1 on average in DMFT compared to TPSC with a factor of 2, resulting in a steeper slope of the self-energy close to  $\omega = 0$  eV. For higher energies the difference between the two approaches becomes much larger, an effect that has already been observed in the single-band TPSC<sup>39</sup> where it was found that TPSC in general underestimates the tail of the self-energy at higher energies, but obtains accurate results for lower energies. Since the local self-energy is the only correction to the electronic structure in the DMFT and local TPSC approximation, this shows that the local TPSC approach is able to capture the local electronic correlations to a high degree.

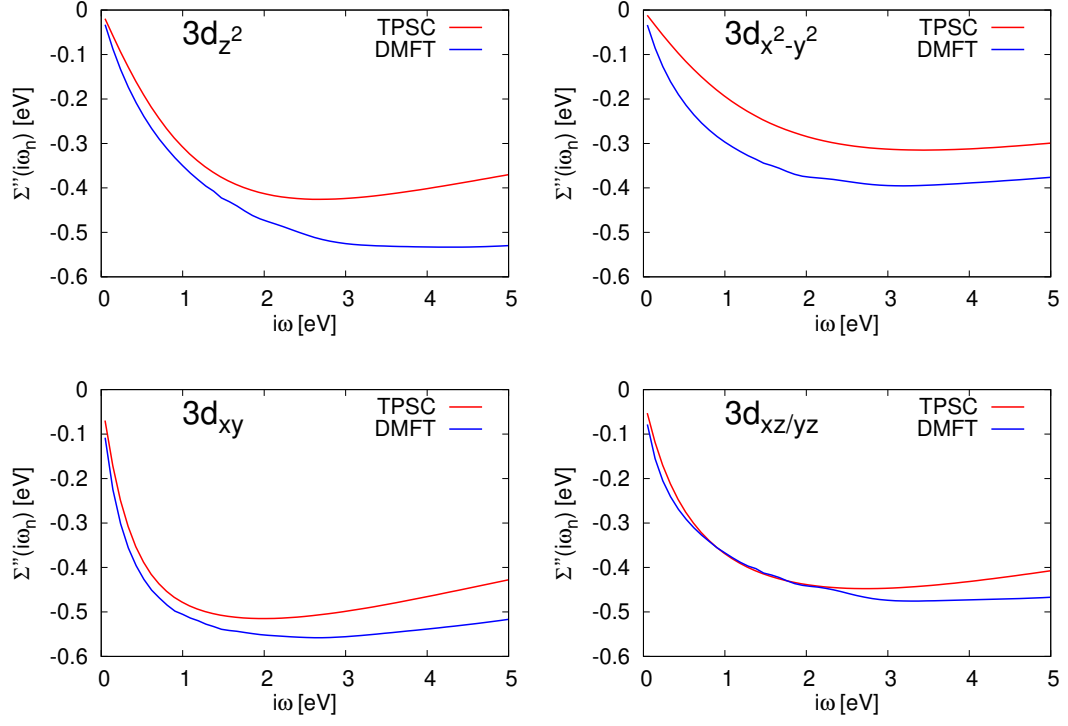


FIG. 4. The imaginary part of the local TPSC self-energy compared to the impurity self-energy obtained from the DMFT approximation. We observe a good agreement in the low-energy part (except for the  $d_{x^2-y^2}$  orbital), which is the most relevant for the low-energy electronic structure like the Fermi surface.

- 
- <sup>44</sup> A. A. Mostofi, J. R. Yates, G. Pizzi, Y.-S. Lee, I. Souza, D. Vanderbilt, and N. Marzari, *Computer Physics Communications* **185**, 2309 (2014).
- <sup>61</sup> T. Miyake, K. Nakamura, R. Arita, and M. Imada, *Journal of the Physical Society of Japan* **79**, 044705 (2010), <https://doi.org/10.1143/JPSJ.79.044705>.
- <sup>43</sup> P. Blaha, K. Schwarz, G. Madsen, D. Kvasnicka, and J. Luitz, *Technische Universitt Wien, Wien* **28** (2001).
- <sup>62</sup> R. Levy, J. LeBlanc, and E. Gull, *Computer Physics Communications* **215**, 149 (2017).
- <sup>21</sup> H. Miao, Z. P. Yin, S. F. Wu, J. M. Li, J. Ma, B.-Q. Lv, X. P. Wang, T. Qian, P. Richard, L.-Y. Xing, X.-C. Wang, C. Q. Jin, K. Haule, G. Kotliar, and H. Ding, *Phys. Rev. B* **94**, 201109 (2016).
- <sup>15</sup> J. Ferber, K. Foyevtsova, R. Valentí, and H. O. Jeschke, *Phys. Rev. B* **85**, 094505 (2012).
- <sup>25</sup> G. Lee, H. S. Ji, Y. Kim, C. Kim, K. Haule, G. Kotliar, B. Lee, S. Khim, K. H. Kim, K. S. Kim, K.-S. Kim, and J. H. Shim, *Phys. Rev. Lett.* **109**, 177001 (2012).
- <sup>63</sup> A. Gaenko, A. Antipov, G. Carcassi, T. Chen, X. Chen, Q. Dong, L. Gamper, J. Gukelberger, R. Igarashi, S. Iskakov, M. Knz, J. LeBlanc, R. Levy, P. Ma, J. Paki, H. Shinaoka, S. Todo, M. Troyer, and E. Gull, *Computer Physics Communications* **213**, 235 (2017).
- <sup>39</sup> Y.M. Vilk and A.-M.S. Tremblay, *J. Phys. I France* **7**, 1309 (1997).